Potent activation of SARM1 by NMN analogue VMN underlies vacor neurotoxicity

Andrea Loreto*[,1,6], Carlo Angeletti[2,6], Jonathan Gilley[1], Peter Arthur-Farraj[1], Elisa Merlini[1], Adolfo Amici[2], Laura M. Desrochers[3,4], Qi Wang[3,5], Giuseppe Orsomando*[,2,7], Michael P. Coleman*[,1,7].

*Corresponding author:

Prof Michael Coleman Email: mc469@cam.ac.uk

*Corresponding author:

Dr Andrea Loreto Email: al850@cam.ac.uk

*Corresponding author:

Dr Giuseppe Orsomando Email: g.orsomando@staff.univpm.it

[1] John van Geest Centre for Brain Repair, Department of Clinical Neurosciences, University of Cambridge, Forvie Site, Robinson Way, CB2 0PY, Cambridge, UK

[2] Department of Clinical Sciences (DISCO), Section of Biochemistry, Polytechnic University of Marche, Via Ranieri 67, Ancona 60131, Italy

[3] Neuroscience, BioPharmaceuticals R&D, AstraZeneca, Waltham, MA, USA

[4] Current address: Vertex Pharmaceuticals, 50 Northern Ave, Boston, MA 02210, USA

[5] Current address: Kymera Therapeutics, 200 Arsenal Yards Blvd, Watertown, MA 02472, USA

[6,7] Equal contribution

ABSTRACT

SARM1 is intensively studied for its role in promoting axon degeneration in injury and disease. We identify VMN, a metabolite of the neurotoxin vacor, as a potent SARM1 activator, an action likely to underlie vacor neurotoxicity in humans. This study provides novel tools to study SARM1 regulation, supports drug discovery, further links programmed axon death to human disease and identifies a new model where axons are permanently rescued.

MAIN

Sterile alpha and TIR motif-containing protein 1 (SARM1) plays a central, pro-degenerative role in programmed axon death (including Wallerian degeneration) [1]. This axon degeneration pathway is activated in a number of neurodegenerative contexts, including in human disease [2–4]. SARM1 has a critical nicotinamide adenine dinucleotide (NAD) cleavage (NADase) activity, which is activated when its upstream regulator and axon survival factor nicotinamide mononucleotide adenylyltransferase 2 (NMNAT2) is depleted or inactive [5–9]. NMNAT2 loss causes accumulation of its substrate nicotinamide mononucleotide (NMN), which we showed promotes axon degeneration [10–13]. NMN is now known to activate SARM1 NADase activity [14]. Given that *Sarm1* deletion confers robust axon protection, and even lifelong protection against lethality caused by NMNAT2 deficiency [15], SARM1 has become a very attractive therapeutic target. Understanding how SARM1 is activated by small molecule regulators will help develop ways to block its activation.

Here we have investigated whether vacor, a disused rodenticide and powerful neurotoxin associated with human peripheral and central nervous system disorders [16,17] and axon degeneration in rats [18], causes activation of programmed axon death. Vacor is metabolised to vacor mononucleotide (VMN) and vacor adenine dinucleotide

(VAD) through a two-step conversion by nicotinamide phosphoribosyltransferase (NAMPT) and NMNAT2 (Fig. S1a). Since VAD inhibits NMNAT2 [19], we reasoned that vacor-induced axon death could be SARM1-dependent.

We first confirmed that VMN and VAD are generated in vacor-treated dorsal root ganglion (DRG) mouse neurons (Fig. S1b) and that these and a second neuron type, superior cervical ganglia (SCG) mouse neurons, exhibit rapid, dose-dependent neurite degeneration (Fig. 1a-d; Fig. S1c-f). Consistent with the proposed toxic role for vacor metabolites, both nicotinamide (NAM), which competes with vacor as a preferred substrate for NAMPT, and the NAMPT inhibitor FK866 (Fig. S1a), delayed vacor-induced neurite degeneration (Fig. S1g-j). Such competition may underlie the use of NAM as a treatment to patients who ingested vacor [16].

As hypothesised, vacor failed to induce degeneration of *Sarm1*$^{-/-}$ DRG and SCG neurites (Fig. 1a-d). This protection was extremely strong with neurites surviving indefinitely even after multiple vacor doses (Fig. S2a,b). *Sarm1*$^{-/-}$ neurites were not only protected from degeneration, but they also continued to grow normally, even with repeated dosing (Fig. 1e,f). This mirrors the permanent rescue and continued growth previously reported in *Nmnat2* null axons [7,15], suggesting complete efficacy in both toxic and inherited types of neuropathy. It also shows vacor neurotoxicity is predominantly SARM1-dependent.

SARM1 levels remained relatively stable following vacor treatment (Fig. S2c-f). We instead confirmed that SARM1 NADase activity is the critical function required for vacor toxicity. Exogenous expression of wild-type human SARM1 (hSARM1) in *Sarm1*$^{-/-}$ SCG neurons restored vacor sensitivity, whereas expression of E642A hSARM1, that lacks NADase activity, did not (Fig. 1g-i; Fig. S2g,h), similar to findings in axotomy [5]. Interestingly, unlike axotomy, activation of the pathway by vacor also

caused SARM1-dependent cell death (Fig. 1i), similar to that previously reported with constitutively active SARM1 [20,21]. To explore this further, we cultured DRG neurons in microfluidic chambers to allow independent manipulation of the axon and soma compartments (Fig. S3a). Local addition of vacor to either compartment directly activated local death of cell bodies and/or neurites. However, while vacor-induced cell death causes eventual secondary neurite degeneration, the reverse was not true: no cell loss was observed after local induction of distal neurite degeneration by vacor.

Activation of SARM1 depletes NAD and generates cADPR in neurons [5,8,9,21]. Based on the previously reported inhibition of NMNAT2 by VAD [19], we initially hypothesised that a rise in NMN, the physiological NMNAT2 substrate and a known activator of SARM1 [10,12,14], stimulates SARM1 activity to trigger vacor-dependent axon death. Surprisingly, while SARM1 activation was confirmed by a dramatic, SARM1-dependent decline in NAD (Fig. 2a,b) and cADPR accumulation (Fig. 2c,d) following vacor administration, NMN did not rise and even fell slightly (Fig. 2a,b). Furthermore, NMN and NAD levels and ratio were not altered in our vacor-treated *Sarm1*$^{-/-}$ neurons (Fig. 2a,b), suggesting that the reported inhibition of NAMPT and NMNAT2 by vacor/VAD [19] does not occur in this context at this drug concentration. Crucially, NMN deamidase, an enzyme that strongly preserves axotomised axons by preventing NMN accumulation (Fig. 3a; Fig. S4a) [10–12], was also unable to protect against vacor toxicity (Fig. 3a,b), even though recombinant NMN deamidase retains its ability to convert NMN to NaMN in the presence of vacor, VMN and VAD (Fig. S4b). Also WLD^{S}, another enzyme that limits NMN accumulation [10], failed to rescue neurons against vacor neurotoxicity (Fig. S4c,d). These data suggest that, in this specific context at least, NMN is not responsible for SARM1 activation.

However, vacor metabolite VMN did accumulate in vacor-treated neurons (Fig. S1b). Given its structural similarity to the endogenous SARM1 activator NMN (Fig. S5a), we hypothesised that VMN might instead directly activate SARM1 leading to cell and axon death. Crucially, we found that VMN potently activates the NADase activity of recombinant hSARM1, even more so than NMN, having a lower Ka and resulting in a greater induction (Fig. 3c). Conversely, VAD only had a weak inhibitory effect on hSARM1 activity (Fig. S5c). Intriguingly, recombinant hSARM1 NADase activity dropped at higher VMN concentrations (Fig. 3c). Notwithstanding the doses of vacor used in this study result in VMN levels in neurons within the activation range of SARM1, this inhibitory action could reveal critical information on how SARM1 activity is regulated. Analysis via best fitting (see equation in Methods) suggests that our data are compatible with two distinct binding sites of VMN on SARM1 and led us to establish binding constants for activation (Ka) and inhibition (Ki) (Fig. 3c).

While NMN activates SARM1 [14] and promotes programmed axon death when NMNAT2 is depleted [10–13], exogenous NMN does not induce degeneration of uninjured neurites [10], probably because it is rapidly converted to NAD when NMNAT2 is present, thereby limiting its accumulation. However, we now show that exogenous application of its analogue, VMN, does induce SARM1-dependent death of uninjured DRG neurites (Fig. 3d,e). This difference likely reflects a combination of VMN being both a more potent activator of SARM1 and it accumulating more because it is not efficiently metabolised by NMNAT2 [19].

VMN-dependent activation of SARM1 being the effector of vacor toxicity is also supported by a number of other findings. First, unlike NMN, VMN is not a substrate of NMN deamidase (Fig. S5d) thus explaining its inability to protect against vacor neurotoxicity (Fig. 3a,b). In addition, VMN is not a substrate of the nuclear isoform

NMNAT1 and is a poor substrate of mitochondrial NMNAT3 [19], so VMN accumulation in cell bodies (Fig. S5e) and subsequent SARM1 activation, as detected by a rise of cADPR in this compartment (Fig. 2d), provides a clear rationale for why vacor administration also causes cell death.

Overall, this study provides clear evidence that direct SARM1 activation by vacor metabolite VMN underlies vacor neurotoxicity. Crucially, the structural and functional similarity between VMN and NMN provides additional support for a key physiological role of NMN in the regulation of SARM1 activity and axon degeneration. Given its greater potency than NMN, we anticipate that VMN and vacor will be important tools for drug discovery projects. Vacor is currently the most effective chemical to directly activate SARM1 and cause neuronal death, eliminating the need for complex axotomy experiments or the use of drugs with non-specific actions. Furthermore, understanding where VMN binds to SARM1, why it activates it more potently than NMN and expanding on VMN activation/inhibition functions should support drug development projects in several ways. One intriguing possibility is that VMN interacts with SARM1 in the auto-inhibitory ARM domain leading to SARM1 activation, and in the catalytic TIR domain, causing inhibition [5,20]. Finally, obtaining full-length SARM1 structures in physiological and active conformations will be essential for rational drug design but, despite recent important developments [22–25], this has proven challenging. However, the possible interaction of VMN with SARM1 could help achieve this.

These data further implicate programmed axon death to human disease. It appears that this degeneration pathway can be aberrantly activated in humans not only by genetic mutation of *NMNAT2* [3,4], but also by SARM1 activation in severe neurotoxicity within hours of vacor ingestion [17]. Although vacor use is banned, this study raises important questions of whether other pesticides or environmental chemicals in use

today also activate programmed axon death. Finally, as vacor causes pancreatic β-cell destruction and diabetes in humans [16], these findings could have broader implications, uncovering a role for SARM1 in the survival of insulin producing cells and aiding research on diabetes.

Fig. 1

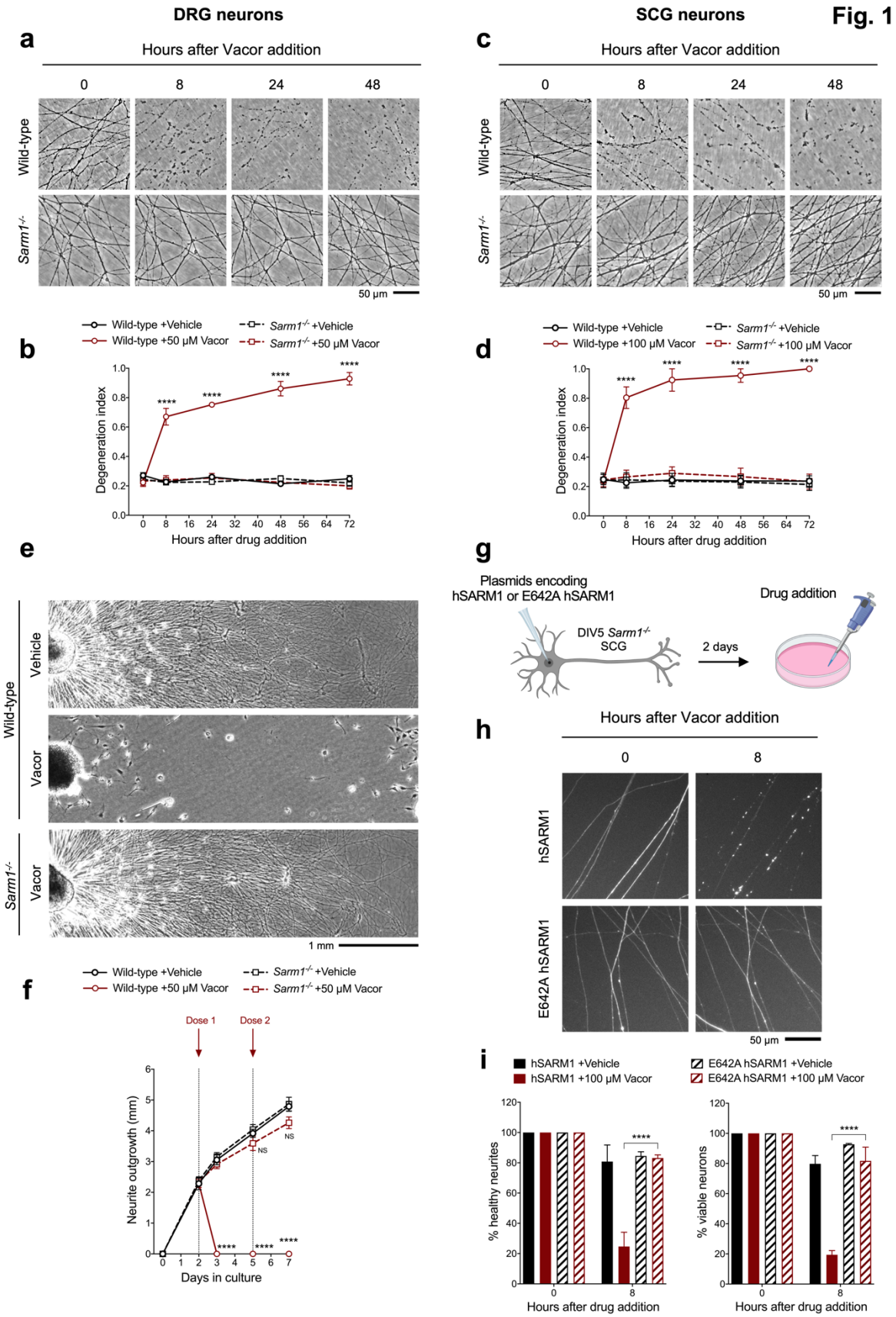

Figure 1. Vacor causes SARM1-dependent neurite and cell death.

(a) Representative images of neurites from wild-type and *Sarm1*$^{-/-}$ DRG (littermates) explant cultures treated with 50 μM vacor. **(b)** Quantification of the degeneration index in experiments described in (a) (Mean ± SEM; n = 4; three-way ANOVA followed by Tukey's multiple comparison test; ****, p<0.0001. Statistical significance shown relative to *Sarm1*$^{-/-}$ +50 μM Vacor). **(c)** Representative images of neurites from wild-type and *Sarm1*$^{-/-}$ SCG explant cultures treated with 100 μM vacor. **(d)** Quantification of the degeneration index in experiments described in (c) (Mean ± SEM; n = 4; three-way ANOVA followed by Tukey's multiple comparison test; ****, p < 0.0001. Statistical significance shown relative to *Sarm1*$^{-/-}$ +100 μM Vacor). **(e)** Representative images of neurite outgrowth at DIV7 from wild-type and *Sarm1*$^{-/-}$ DRG explant cultures treated with 50 μM vacor or vehicle. Multiple doses of vacor or vehicle were added at DIV2 and DIV5. **(f)** Quantification of neurite outgrowth in (e) (Mean ± SEM; n = 5; three-way ANOVA followed by Tukey's multiple comparison test; ****, p < 0.0001; NS, not-significant. Statistical significance shown relative to Wild-type +Vehicle). **(g)** Schematic representation of the experimental design for (h) ('Created with BioRender'). **(h)** Representative images of neurites from *Sarm1*$^{-/-}$ SCG dissociated neurons co-injected with plasmids encoding wild-type or E642A hSARM1 and DsRed (to label neurites) and treated with 100 μM vacor. **(i)** Quantification of healthy neurites and viable neurons in experiments in (h) is shown as a percentage relative to 0 hr (time of drug addition) (Mean ± SEM; n = 3; three-way ANOVA followed by Tukey's multiple comparison test; ****, p < 0.0001).

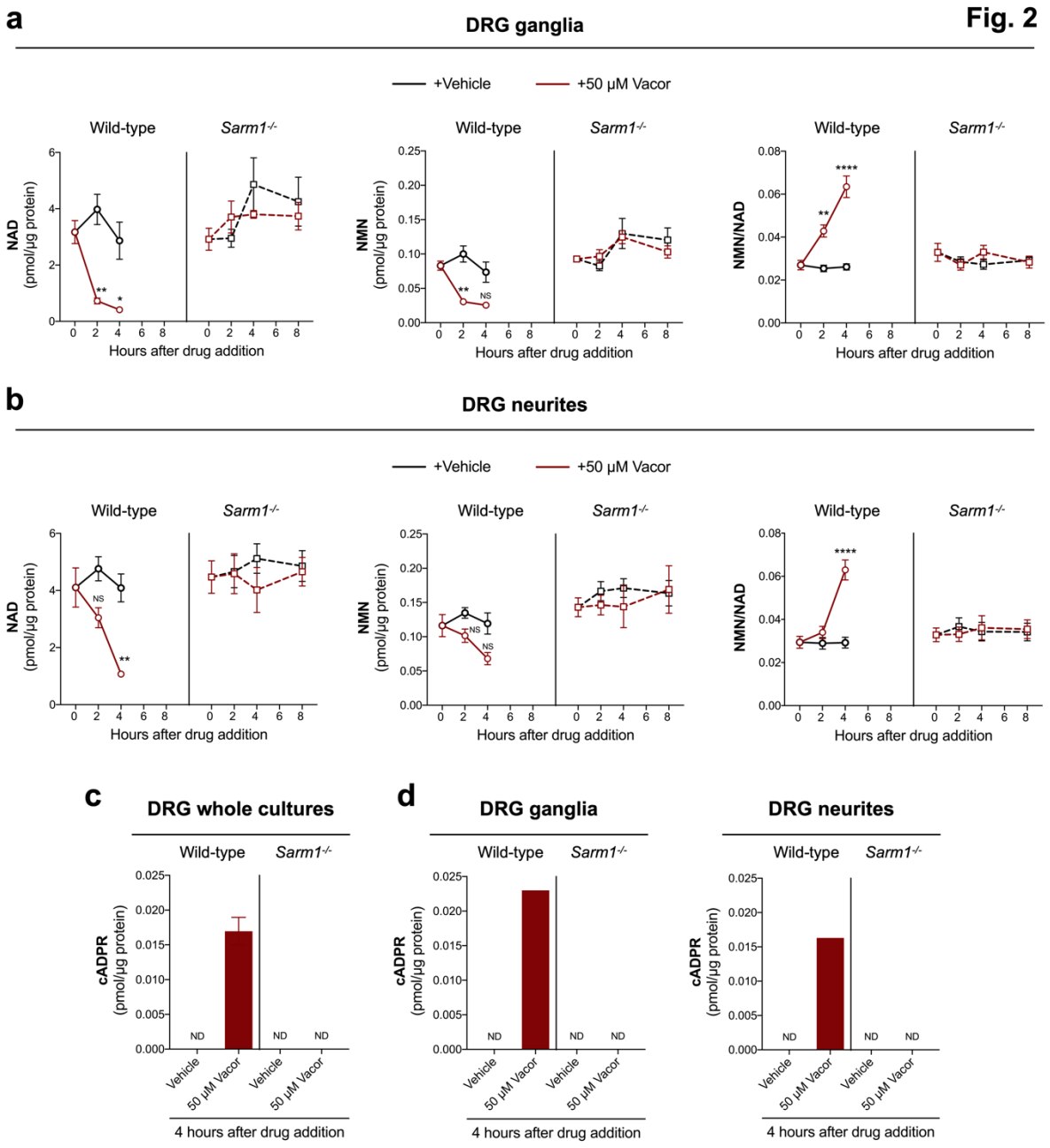

Figure 2. Activation of SARM1 following vacor treatment leads to NAD loss and cADPR accumulation.

(a,b) NMN and NAD levels and NMN/NAD ratio in ganglia (a) and neurite (b) fractions from wild-type and *Sarm1*$^{-/-}$ DRG explant cultures at the indicated time points after 50 μM vacor or vehicle treatment (Mean ± SEM; n = 4; three-way ANOVA followed by Tukey's multiple comparison test; ****, $p < 0.0001$; **, $p < 0.01$; *, $p < 0.05$; NS, not-significant). **(c)** cADPR levels in wild-type and *Sarm1*$^{-/-}$ DRG whole explant cultures (neurites and cell bodies) 4 hr after 50 μM vacor or vehicle treatment. cADPR levels were consistently above the detection limit (~1 fmol/μg protein) only in wild-type DRG

explant cultures treated with vacor (Mean ± SEM; n = 3; ND, not-detectable). **(d)** A single analysis of cADPR levels in ganglia and neurite fractions from wild-type and *Sarm1*$^{-/-}$ DRG explant cultures 4 hr after 50 μM vacor or vehicle treatment (n = 1).

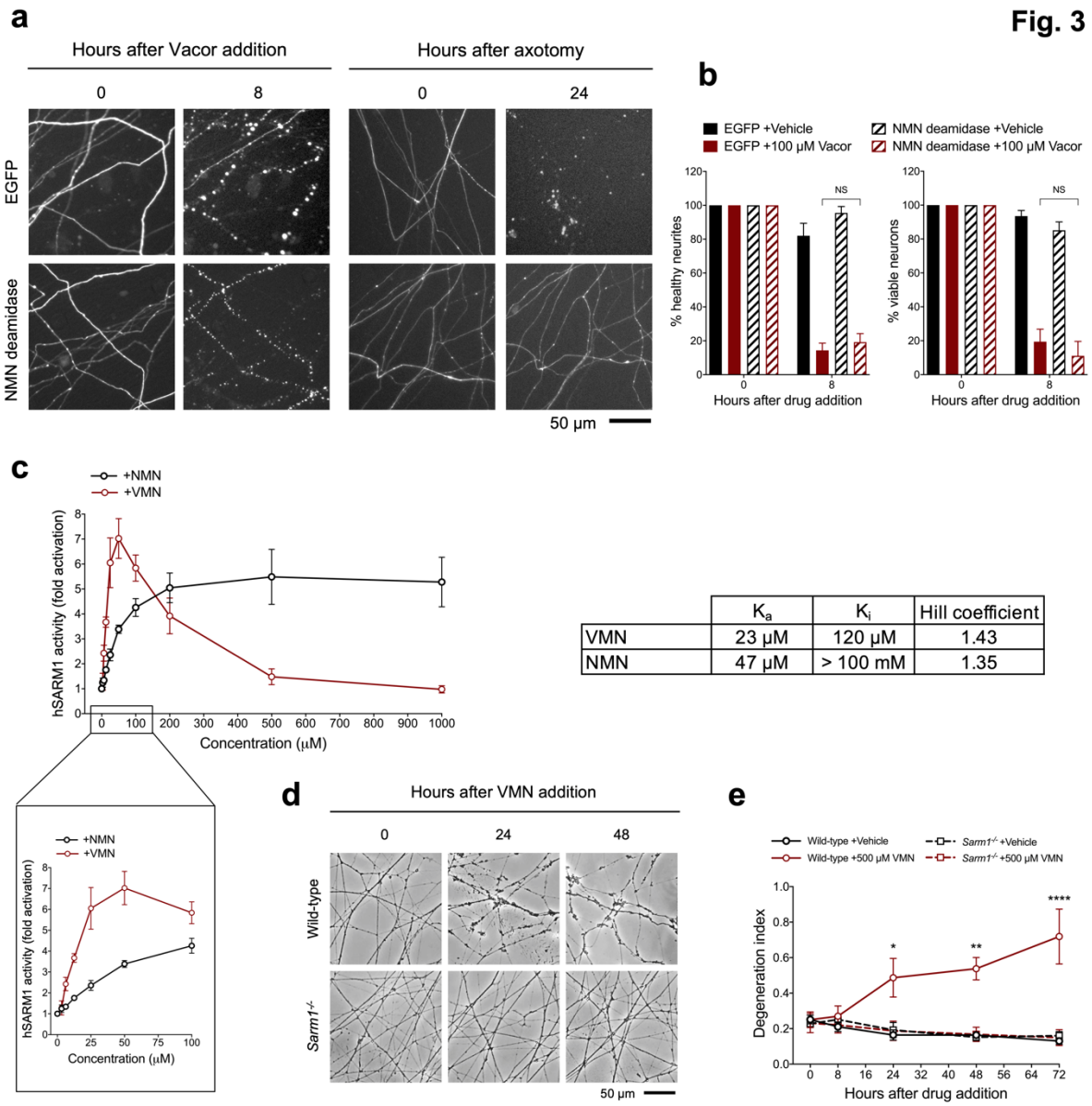

	K_a	K_i	Hill coefficient
VMN	23 µM	120 µM	1.43
NMN	47 µM	> 100 mM	1.35

Figure 3. VMN potently activates SARM1 and causes neurite degeneration.

(a) Representative images of neurites from *Sarm1*$^{-/-}$ SCG dissociated neurons co-injected with plasmids encoding hSARM1, EGFP or EGFP-NMN deamidase and DsRed (to label neurites) and treated with 100 µM vacor. As an experimental control, *Sarm1*$^{-/-}$ SCG dissociated neurons injected with the same injection mixtures were axotomised. As expected, neurites expressing NMN deamidase were still intact 24 hr after axotomy. **(b)** Quantification of healthy neurites and viable neurons in experiments in (a) is shown as a percentage relative to 0 hr (time of drug addition) (Mean ± SEM; n = 3; three-way ANOVA followed by Tukey's multiple comparison test; NS, not-significant). **(c)** Fold change of NADase activity of purified, recombinant hSARM1 in the presence of NMN and VMN (Mean ± SEM; n = 3). hSARM1 average basal activity

is 18.12 ± 3.02 milliU/mg (fold activation = 1). Rates are relative to controls measured with 250 μM NAD alone. Both NMN and VMN, once added to each reaction mixture, were not consumed during incubation. Experimental data were fitted to the modified Michaelis-Menten equation in Methods to calculate the shown kinetic parameters (table). Hill coefficients for NMN and VMN indicate positive cooperativity binding in both cases. Best fitting also revealed a K_m for NAD of 70 μM. **(d)** Representative images of neurites from wild-type and *Sarm1*$^{-/-}$ DRG (littermates) explant cultures treated with 500 μM VMN. **(e)** Quantification of the degeneration index in experiments described in (d) (Mean ± SEM; n = 3; three-way ANOVA followed by Tukey's multiple comparison test; ****, $p < 0.0001$; **, $p < 0.01$; *, $p < 0.05$. Statistical significance shown relative to *Sarm1*$^{-/-}$ +500 μM VMN).

Fig. S1

a

b

4 hours after Vacor addition

	pmol/µg protein	SEM +/-
Vacor	2.10	0.281
VMN	0.17	0.039
VAD	0.14	0.017

c

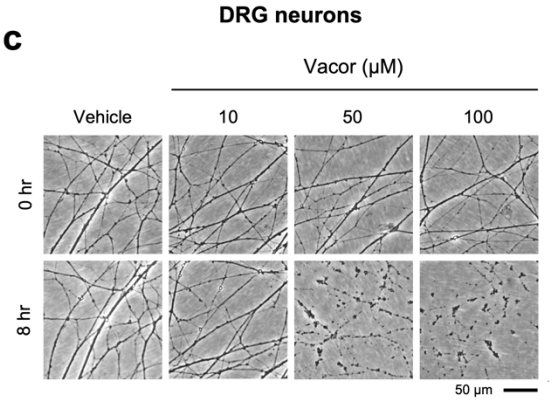

d

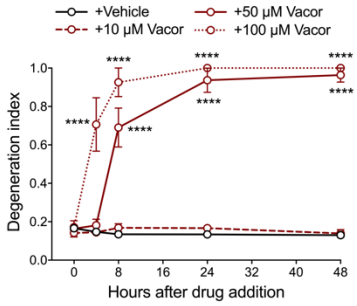

e

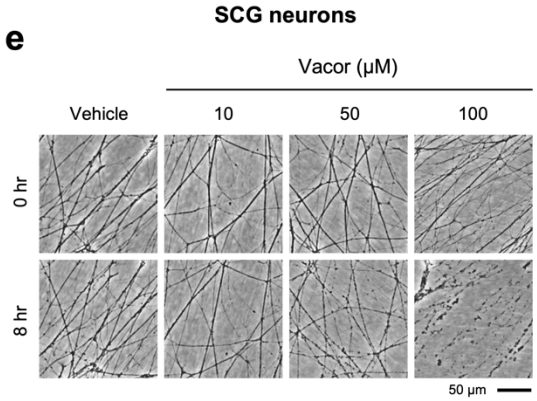

f

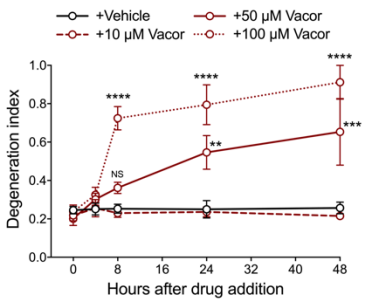

g

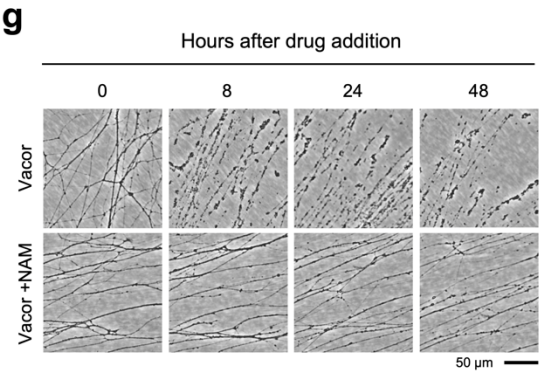

h

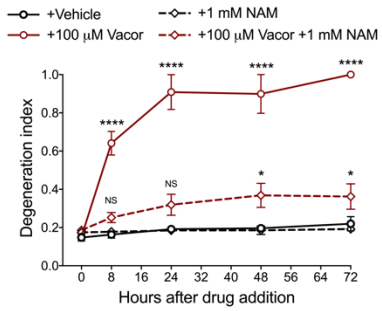

i

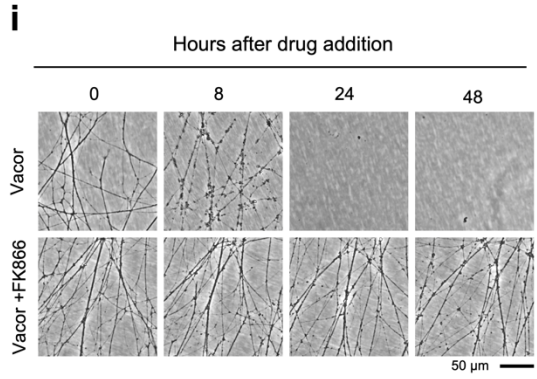

j

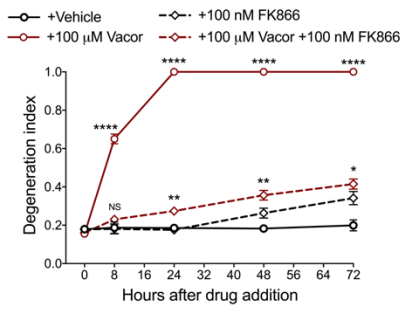

Figure S1. Vacor causes neurite degeneration in primary mouse neurons.

(a) Schematic representation of vacor conversion into VMN and VAD by NAMPT and NMNAT2, respectively. VAD has been reported to inhibit NMNAT2 [19]. Vacor competes with NAM for NAMPT. High doses of NAM or inhibition of NAMPT with FK866 prevent vacor conversion into downstream metabolites (NAM, nicotinamide; NaMN, nicotinic acid mononucleotide; NMN, nicotinamide mononucleotide; NAD, nicotinamide adenine dinucleotide; NAMPT, nicotinamide phosphoribosyltransferase; NMNAT2, nicotinamide mononucleotide adenylyltransferase 2; VMN, vacor mononucleotide; VAD, vacor adenine dinucleotide). **(b)** Vacor, VMN and VAD levels in wild-type DRG whole explant cultures (neurites and cell bodies) 4 hr after 50 μM vacor treatment (Mean ± SEM; n = 3). **(c)** Representative images of neurites from wild-type DRG explant cultures treated with 10, 50, 100 μM vacor or vehicle. **(d)** Quantification of the degeneration index in experiments described in (c) (Mean ± SEM; n = 3; two-way ANOVA followed by Tukey's multiple comparison test; ****, $p < 0.0001$. Statistical significance shown relative to +Vehicle). **(e)** Representative images of neurites from wild-type SCG explant cultures treated with 10, 50, 100 μM vacor or vehicle. **(f)** Quantification of the degeneration index in experiments described in (c) (Mean ± SEM; n = 3; two-way ANOVA followed by Tukey's multiple comparison test; ****, $p < 0.0001$; ***, $p < 0.001$; **, $p < 0.01$; NS, not-significant. Statistical significance shown relative to +Vehicle). **(g)** Representative images of neurites from wild-type SCG explant cultures treated with 100 μM vacor or 100 μM vacor + 1 mM NAM. **(h)** Quantification of the degeneration index in experiments described in (g) (Mean ± SEM; n = 3; two-way ANOVA followed by Tukey's multiple comparison test; ****, $p < 0.0001$; *, $p < 0.05$; NS, not-significant. Statistical comparisons shown are: +100 μM Vacor vs +100 μM Vacor +1 mM NAM and +1 mM NAM vs +100 μM Vacor +1 mM NAM). **(i)** Representative images of neurites from wild-type SCG explant cultures treated with 100 μM vacor, 100 nM FK866 or vehicle. **(j)** Quantification of the degeneration index in experiments described in (i) (Mean ± SEM; n = 3; two-way ANOVA followed by Tukey's multiple comparison test; ****, $p < 0.0001$; **, $p < 0.01$; *, $p < 0.05$; NS, not-significant. Statistical comparisons shown are: +100 μM Vacor vs +100 μM Vacor +100 nM FK866 and +100 nM FK866 vs +100 μM Vacor +100 nM FK866).

Fig. S2

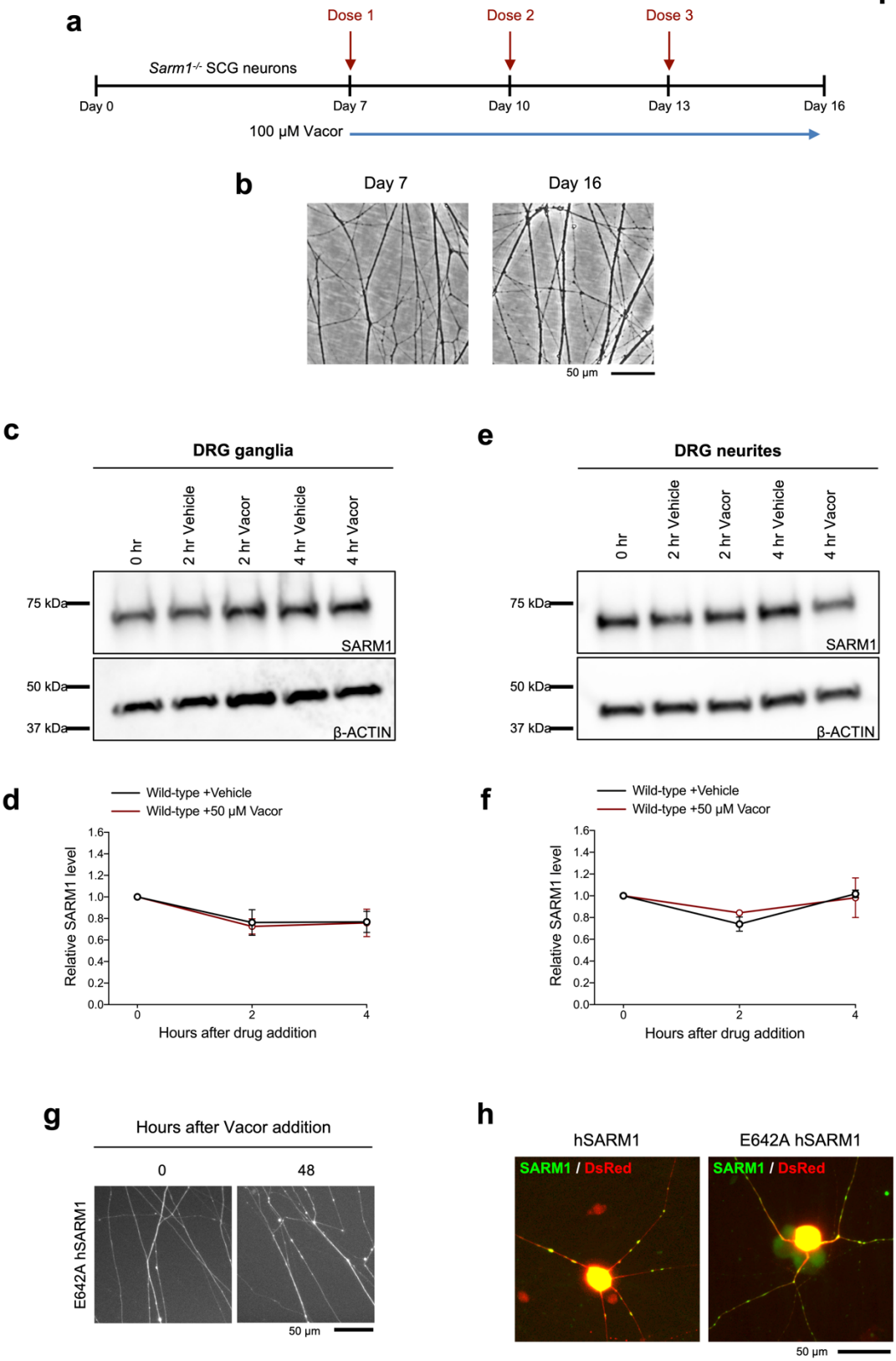

Figure S2. Long-term survival of *Sarm1*$^{-/-}$ SCG neurites following multiple vacor doses.

(a) Schematic representation of the experimental design. *Sarm1*$^{-/-}$ SCG explant cultures were treated with 100 μM vacor at DIV7. Multiple doses of vacor were administered by replacing the media every 3 days with fresh media containing vacor. **(b)** Representative images of neurites from *Sarm1*$^{-/-}$ SCG explant cultures showing no degeneration at 16 days, after treatment with three doses of 100 μM vacor. **(c)** Representative immunoblots of the ganglia fraction from wild-type DRG explant cultures at the indicated time points after 50 μM vacor or vehicle probed for SARM1 and β-ACTIN (loading control). **(d)** Quantification of normalised SARM1 level (to β-ACTIN) is shown, with data presented relative to 0 hr (Mean ± SEM; n = 4; two-way ANOVA followed by Tukey's multiple comparison test). **(e)** Representative immunoblots of the neurite fraction from wild-type DRG explant cultures at the indicated time points after 50 μM vacor or vehicle probed for SARM1 and β-ACTIN (loading control). **(f)** Quantification of normalised SARM1 level (to β-ACTIN) is shown, with data presented relative to 0 hr (Mean ± SEM; n = 4; two-way ANOVA followed by Tukey's multiple comparison test). **(g)** Representative images showing long-term survival of neurites from *Sarm1*$^{-/-}$ SCG dissociated neurons co-injected with plasmids encoding E642A hSARM1 and DsRed (to label neurites) and treated with 100 μM vacor. **(h)** Representative images showing expression of both wild-type and E642A hSARM1 for microinjection experiments in (Fig. 1g-i). The absence of vacor-induced toxicity in neurons expressing E642A hSARM1 is therefore due to loss of enzymatic activity rather than the lack of protein expression.

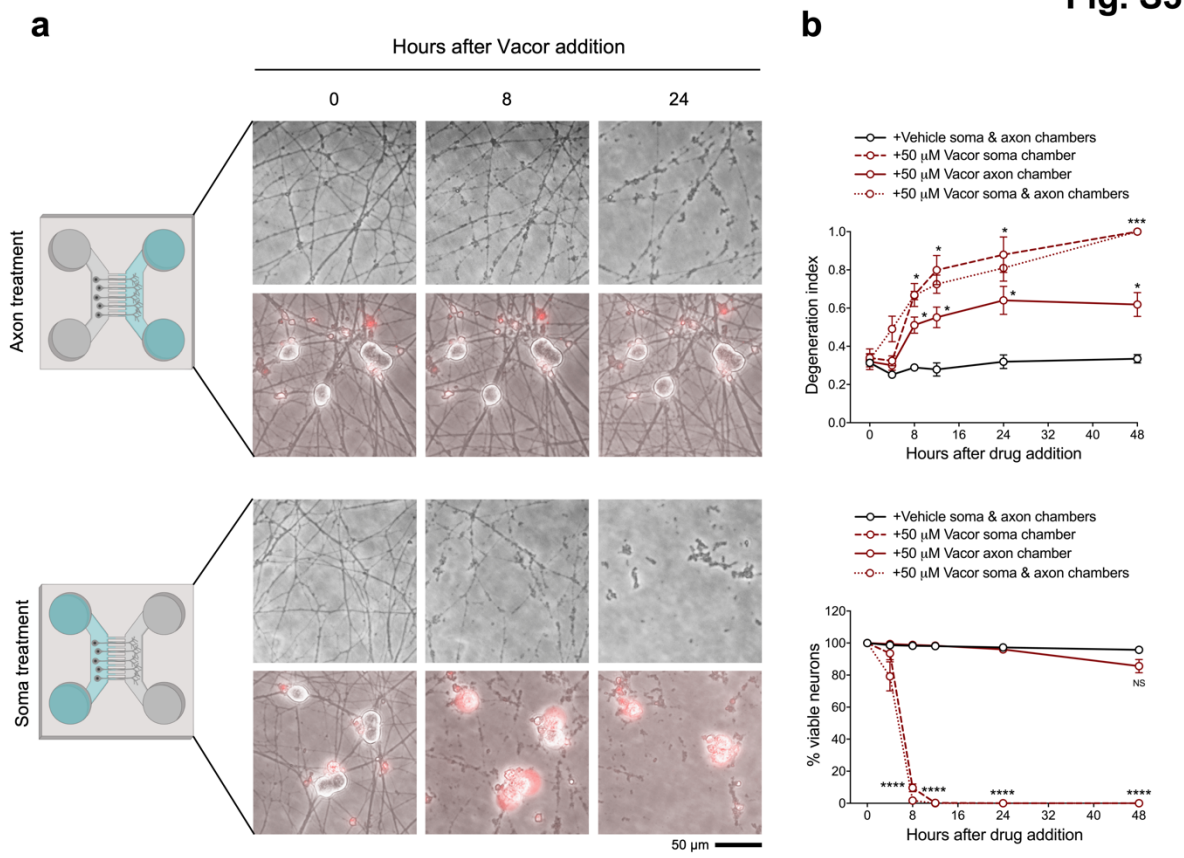

Figure S3. Local death of neurites and cell bodies caused by vacor.

(a) Representative images of neurites and cell bodies from wild-type DRG dissociated neurons cultured in microfluidic chambers and treated with 50 µM vacor or vehicle ('Created with BioRender'). **(b)** Quantification of the degeneration index and viable neurons (shown as a percentage relative to 0 hr) in experiments described in (a) (Mean ± SEM; n = 4; two-way ANOVA followed by Tukey's multiple comparison; ***, $p < 0.001$; *, $p < 0.05$. Statistical significance shown relative to +Vehicle soma & axon chambers).

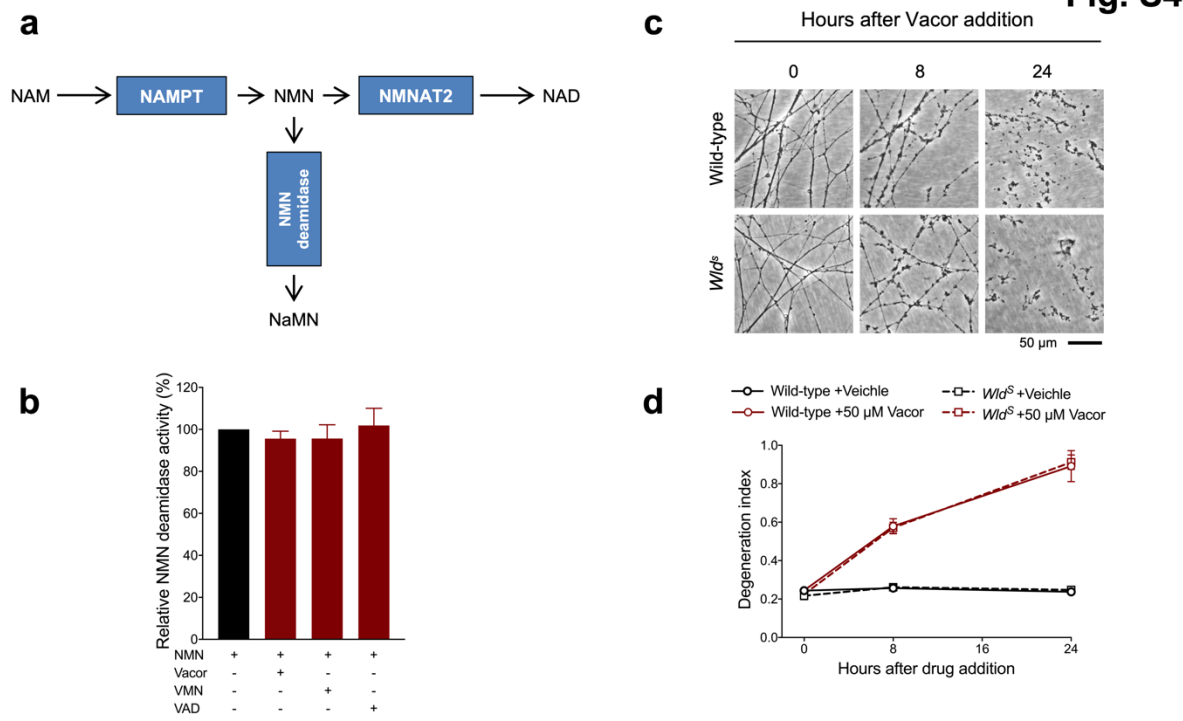

Figure S4. Effect of vacor, VMN and VAD on recombinant NMN deamidase activity and lack of protection after vacor treatment in *Wld^S* neurons.

(a) Schematic representation of NAD biosynthetic pathway from NAM and the side reaction catalysed by bacterial NMN deamidase which prevents accumulation of the NMN intermediate. **(b)** Relative activity (%) (NMN conversion into NaMN) of purified, recombinant NMN deamidase in the presence of vacor, VMN and VAD (all 250 µM) (Mean ± SD; n = 2). **(c)** Representative images of neurites from wild-type and *Wld^S* DRG explant cultures treated with 50 µM vacor. **(d)** Quantification of the degeneration index in experiments described in (c) (Mean ± SEM; n = 4; three-way ANOVA followed by Tukey's multiple comparison test).

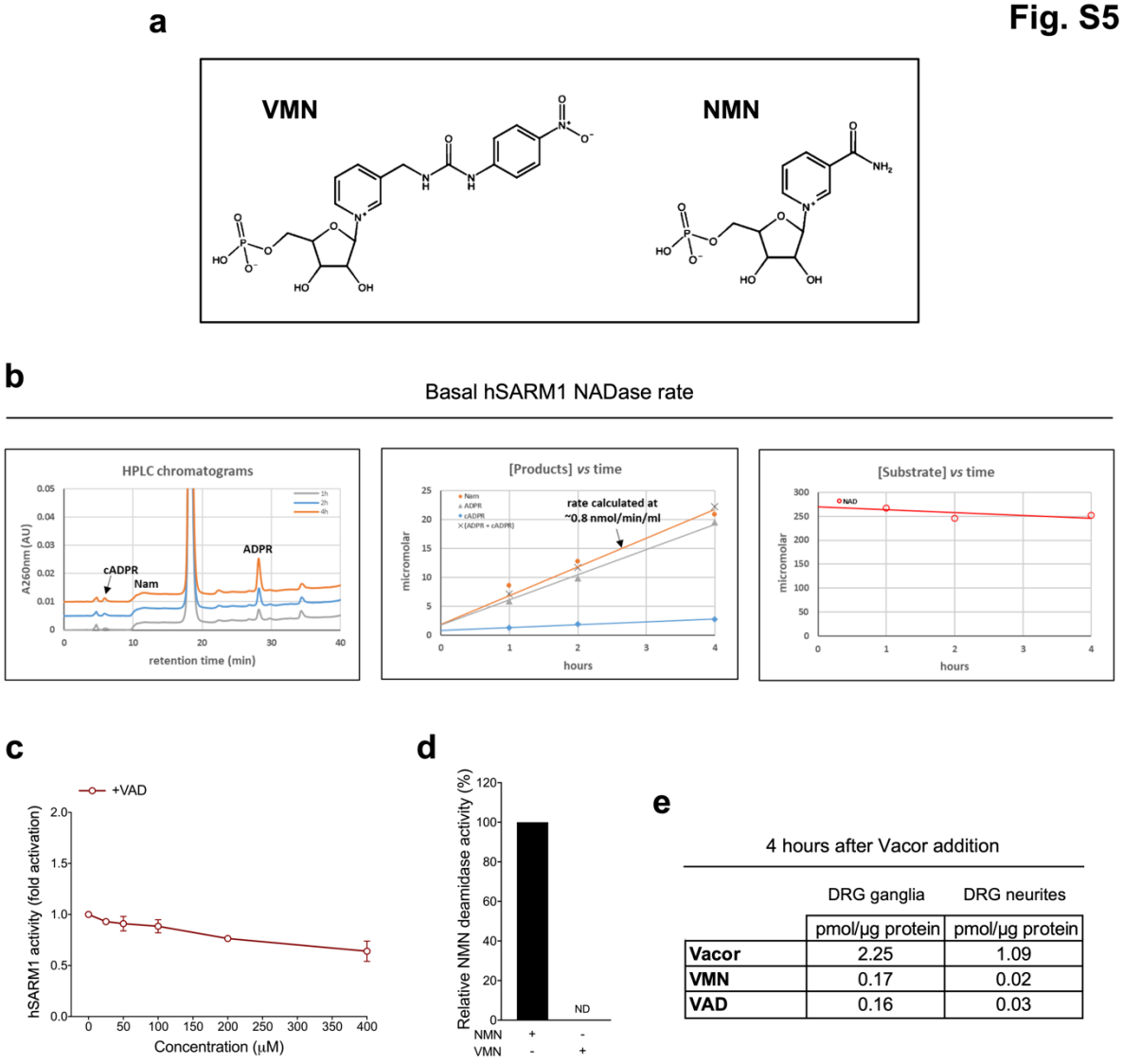

	DRG ganglia	DRG neurites
	pmol/μg protein	pmol/μg protein
Vacor	2.25	1.09
VMN	0.17	0.02
VAD	0.16	0.03

Figure S5. Representative basal NADase rate of recombinant hSARM1.

(a) Chemical structures of the two pyridine 5' mononucleotides VMN and NMN. **(b)** Representative chromatogram and graphs showing basal NADase activity of purified, recombinant hSARM1 (40 μg/ml). The formed products after separation (left panel) are quantified by peak-area integration and evaluated for linearity (middle panel). The NADase rate is calculated from accumulating products ADPR and cADPR (middle panel). In every experiment, the sum of ADPR and cADPR fully matched the amount of NAM formed (middle panel) as well as the amount of NAD consumed (right panel). **(c)** Fold change of NADase activity of purified, recombinant hSARM1 in the presence of VAD (Mean ± SD; n = 2). Rates are relative to control measured with 250 μM NAD alone. VAD, once added to the reaction mixture, was not consumed during incubation. **(d)** Relative activity (%) of purified, recombinant NMN deamidase with VMN as a substrate. NMN or VMN were assayed at 250 μM (Mean ± SD; n = 2). **(e)** A single

analysis of vacor, VMN and VAD levels in wild-type DRG ganglia and neurite fractions 4 hr after 50 μM vacor treatment (n = 1).

a

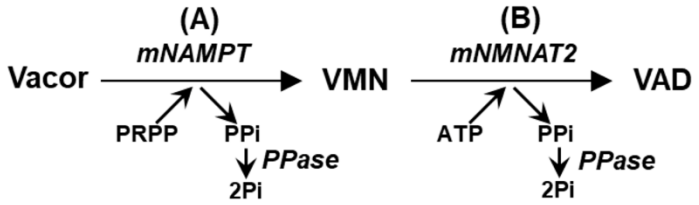

b

	Mix (A) for VMN		Mix (A+B) for VAD	
	ml	**final [ ]**	**ml**	**final [ ]**
H_2O	12.8	-	12.2	
HEPES/NaOH 1 M, pH 7.5	0.75	50 mM	0.75	50 mM
$MgCl_2$ 1 M	0.30	20 mM	0.30	20 mM
ATP 100 mM	0.15	1 mM	0.30	2 mM
PRPP 50 mM	0.15	0.5 mM	0.15	0.5 mM
Vacor 9 mM	0.50	0.3 mM	0.50	0.3 mM
mNAMPT wild type ~0.25 U/ml	0.35 (*)	~6 mU/ml	0.35 (*)	~0.006 U/ml
mNMNAT2 wild type ~2.5 U/ml	-	-	0.44 (*)	~0.075 U/ml
Yeast PPase Sigma >2 KU/ml	-	-	0.01	>1.33 U/ml
Final mix	15 ml		15 ml	
Incubation settings	2-3 hr at 37 °C		Overnight (~19 hr) at 30 °C	

(*) Reagent(s) added to start the reactions.

c **d**

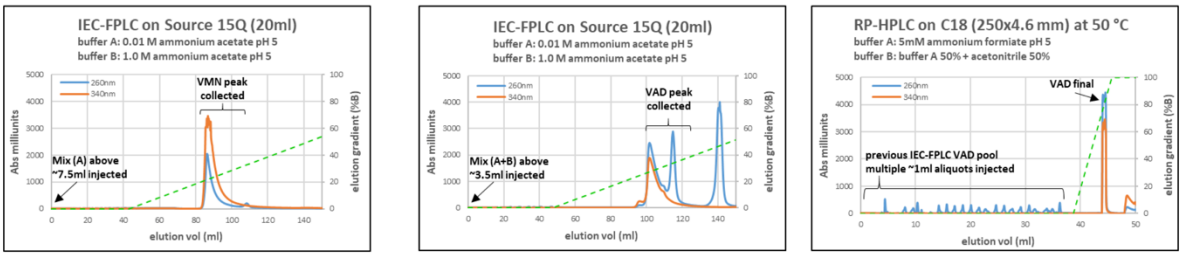

Figure S6. VMN and VAD synthesis and purification.

(a) Scheme of the reactions for VMN and VAD synthesis. **(b)** List of reagents used in mix (A) for VMN synthesis and mix (A+B) for VAD synthesis. **(c)** Representative IEC-FPLC purification of VMN from a typical mix (A). **(d)** Representative IEC-FPLC + RP-HPLC purification of VAD from a typical mix (A+B). Starting from vacor, typical conversion yields obtained via this protocol were 70% for VMN and 50% or less for VAD that required two chromatographic steps for purification.

METHODS

All studies conformed to the institution's ethical requirements in accordance with the 1986 Animals (Scientific Procedures) Act.

Primary neuronal cultures

C57BL/6Babr, *Sarm1*$^{-/-}$ and *Wld*^{S} DRG ganglia were dissected from E13.5-E14.5 mouse embryos and SCG ganglia were dissected from postnatal day 0-2 mouse pups. Littermates from *Sarm1*$^{+/-}$ crosses were used when possible, as indicated in figure legends. Explants were cultured in 35 mm tissue culture dishes pre-coated with poly-L-lysine (20 µg/ml for 1 hr; Merck) and laminin (20 µg/ml for 1 hr; Merck) in Dulbecco's Modified Eagle's Medium (DMEM, Gibco) with 1% penicillin/streptomycin, 50 ng/ml 2.5S NGF (all Invitrogen) and 2% B27 (Gibco). 4 µM aphidicolin (Merck) was used to reduce proliferation and viability of small numbers of non-neuronal cells. For cultures of dissociated SCG neurons, *Sarm1*$^{-/-}$ SCG ganglia were incubated in 0.025% trypsin (Merck) in PBS (without $CaCl_2$ and $MgCl_2$) (Merck) for 30 min followed by incubation with 0.2% collagenase type II (Gibco) in PBS for 20 min. Ganglia were then gently dissociated using a pipette. Dissociated neurons were plated in a poly-L-lysine and laminin-coated area of ibidi µ-dishes (Thistle Scientific) for microinjection experiments. Dissociated cultures were maintained as explant cultures except that B27 was replaced with 10% fetal bovine serum (Merck) and 2.5S NGF was lowered to 30 ng/ml. Culture media was replenished every 3 days. For most experiments, neurites were allowed to extend for 7 days before treatment.

Drug treatments

For most experiments, DRG and SCG neurons were treated at day *in vitro* (DIV) 7 with vacor (Greyhound chromatography) or vehicle (H_2O with 4% 1N HCl), and VMN or vehicle (H_2O) just prior to imaging (time 0 hr). When used, FK866 (kind gift of Prof

Armando Genazzani, University of Novara) and NAM (Merck) were added at the same time as vacor. For neurite outgrowth and long-term survival assays, multiple doses of vacor or vehicle were added by replacing media with fresh media containing the drugs at the timepoints indicated in the figure. The drug concentrations used are indicated in the figures and figure legends. Vacor was dissolved in H_2O with 4% 1N HCl; quantitation of the dissolved stock was performed spectrophotometrically (ε_{340nm} 17.8 $mM^{-1}cm^{-1}$).

Acquisition of phase contrast images and quantification of neurite degeneration and outgrowth

Phase contrast images were acquired on a DMi8 upright fluorescence microscope (Leica microsystems) coupled to a monochrome digital camera (Hammamatsu C4742-95). The objectives used were NPLAN 5X/0.12 for neurite outgrowth assays and HCXPL 20X/0.40 CORR for neurite degeneration assays. Radial outgrowth was determined by taking the average of two measurements of representative neurite outgrowth for each ganglion at DIV2-3-5-7. Measurements were made from overlapping images of the total neurite outgrowth. For neurite degeneration assays, the degeneration index was determined using an ImageJ plugin [26]. For each experiment, the average was calculated from three fields per condition; the total number of experiments is indicated in the figure legends.

Microinjection and quantification of % of healthy neurites and viable neurons

DIV5 dissociated *Sarm1*$^{-/-}$ SCG neurons were microinjected using a Zeiss Axiovert S100 microscope with an Eppendorf FemtoJet microinjector and Eppendorf TransferMan® micromanipulator. Plasmids were diluted in 0.5X PBS (without $CaCl_2$and $MgCl_2$) and filtered using a Spin-X filter (Costar). The mix was injected directly into the nuclei of SCG neurons using Eppendorf Femtotips. Injected plasmids

were allowed to express for 2 days before vacor or vehicle treatment and axotomy. Plasmids were injected at the following concentrations: 2.5 (Fig. 1g-i) or 10 (Fig. 3a,b) ng/µl (untagged) hSARM1 and 2.5 ng/µl E642A hSARM1 expression constructs (pCMV-Tag2 backbone), 30 ng/µl EGFP-NMN deamidase expression construct (pEGFP-C1 backbone), 30 ng/µl pEGFP-C1, 40 (Fig. 1g-h) and 70 (Fig. 3a,b) ng/µl pDsRed2-N1. To check for expression (Fig. S2h), untagged and E642A hSARM1 constructs and pDsRed2-N1 were injected at 25 ng/µl; neurons were then fixed in 4% PFA (Merck) and immunostained with mouse monoclonal anti-SARM1 primary antibody [27] followed by Alexa Fluor 488 anti-mouse secondary antibody (Thermo Fisher Scientific). Fluorescence microscopy images were acquired on a DMi8 upright fluorescence microscope (Leica microsystems) coupled to a monochrome digital camera (Hammamatsu C4742-95). The objective used was HCXPL 20X/0.40 CORR. Numbers of morphologically normal and continuous DsRed labelled neurites and morphologically normal cell bodies were counted in the same field at the indicated timepoints after vacor or vehicle treatment. For each experiment, the average was calculated from three fields per condition; the total number of experiments is indicated in the figure legends. The percentage of healthy neurites and viable neurons remaining relative to the first time point was determined.

Microfluidic cultures

Dissociated DRG neurons were plated in microfluidic chambers (150 µm barrier, XONA microfluidics). Cell suspension was pipetted into each side of the upper channel of the microfluidic device. On DIV7, a difference of 100 µl of media between chambers was introduced and drugs were added to the compartment with the lower hydrostatic pressure. To calculate the % of viable neurons, 1 µg/ml propidium iodide (PI) (Thermo Fisher Scientific) was added to the media 15 min before drug addition. Phase contrast

and fluorescence microscopy images were acquired on a DMi8 upright fluorescence microscope (Leica microsystems) coupled to a monochrome digital camera (Hammamatsu C4742-95). The objective used was HCXPL 20X/0.40 CORR. For each experiment, the degeneration index was calculated from the average of two distal fields of neurites per condition, whereas the % of viable neurons remaining relative to the first time point was calculated from the average of three fields of cell bodies (staining positive for PI) per condition; the total number of experiments is indicated in the figure legends.

Determination of NMN, NAD, cADPR, vacor, VMN and VAD tissue levels

Following treatment with vacor or vehicle, DIV7 wild-type and *Sarm1*$^{-/-}$ DRG ganglia were separated from their neurites with a scalpel. Neurite and ganglia (containing short proximal neurite stumps as well as cell bodies) fractions were washed in ice-cold PBS and rapidly frozen in dry ice and stored at −80 °C until processed. Tissues were ground in liquid N_2 and extracted in $HClO_4$ by sonication followed by neutralisation with K_2CO_3. NMN and NAD were subsequently analysed by spectrofluorometric HPLC analysis after derivatization with acetophenone [28]. Vacor, VMN and VAD were determined in DRG whole explant cultures by ion pair C18-HPLC chromatography, as previously described [19]. cADPR levels were determined in DRG whole explant cultures using a cycling assay, as previously described [29]. A single analysis of vacor, VMN, VAD and cADPR levels was performed in DRG neurite and ganglia fractions independently, which was not further repeated due to the low basal levels of these metabolites and the amount of cellular material needed for this type of analysis. Metabolites levels were normalised to protein levels quantified with the Bio-Rad Protein Assay (Bio-Rad) on formiate-resuspended pellets from the aforementioned $HClO_4$ extraction.

VMN and VAD synthesis and purification

VMN and VAD were synthesized as previously reported [19] with minor changes. Vacor was either phosphoribosylated *in vitro* by murine NAMPT (mNAMPT) into VMN or phosphoribosylated by mNAMPT and adenylated by murine NMNAT2 (mNMNAT2) into VAD. The scheme of these reactions and the reaction mixtures are shown in (Fig. S6a,b). Inorganic yeast pyrophosphatase (PPase), phosphoribosyl 1-pyrophosphate (PRPP) and adenosine triphosphate (ATP) were all from (Merck). Recombinant mNAMPT and mNMNAT2 were purified as previously described [30,31]. Following incubation, reaction mixtures (A) for VMN and (A+B) for VAD (Fig. S6b) were stopped by rapid cooling on ice and kept refrigerated until injection for purification. Next, the VMN and VAD obtained were purified by FPLC under volatile solvents and lyophilised. Briefly, a preparative IEC chromatography was carried out on AKTA Purifier onto the anion exchanger resin Source 15Q (GE HealthCare, 20 ml volume). The column was equilibrated at room temperature (~25 °C), at 5 ml/min. After injection of the two mixtures above, a linear gradient elution was applied by mixing the two volatile buffers as indicated. The eluate was monitored at wavelengths of 260 nm and 340 nm (optimal for vacor nucleotides), and both VMN and VAD peaks were collected (Fig. S6c,d). Next, an additional chromatography was performed by HPLC onto a RP C18 column (Varian, 250 x 4.6 mm, 5µ particles) heated at 50 °C to obtain a pure VAD stock. The equilibration in such case was carried out at 1 ml/min in ammonium formiate buffer; this was followed by multiple injections of the previously collected IEC pool of VAD (~1 ml each), and elution by a linear gradient of increasing acetonitrile in the buffer. The eluate was monitored again at wavelengths 260 nm and 340 nm and the VAD peak was collected (Fig. S6d). After lyophilisation, dry pellets were stored at -80 °C. The resulting VMN and VAD lyophilised powders were 100% pure. Their quantitation after resuspension in H_2O was performed spectrophotometrically (ε_{340nm} of 17.8 $mM^{-1}cm^{-1}$).

Recombinant hSARM1 purification

Recombinant, full-length C-terminal Flag-tagged human SARM1 (hSARM1-Flag) was expressed in HEK293T cells and purified by immunoprecipitation. HEK cells at 50-70% confluence were transfected with hSARM1-Flag expression construct (pLVX-IRES-ZsGreen vector backbone) using Lipofecatmine 2000 (Thermo Fisher Scientific). To boost hSARM1-Flag expression media was supplemented with 2 mM nicotinamide riboside (prepared from Tru Niagen® capsules by dissolving the contents and passing through a 0.22 µm filter) at the time of transfection. After 24 hr cells were collected and washed in cold PBS 24 hr and lysed for 10 min with trituration by pipetting and repeated vortexing in ice-cold KHM buffer (110 mM potassium acetate, 20 mM HEPES pH 7.4, 2 mM $MgCl_2$, 0.1 mM digitonin) with cOmplete™, Mini, EDTA-free protease inhibitor cocktail (Roche). After centrifugation for 5 min at 3000 rpm in a chilled microfuge, the supernatant was collected and diluted to 1 µg/µl in KHM buffer after determination of its protein concentration by Pierce BCA assay (Thermo Fisher Scientific). For immunoprecipitation, 1 ml of extract was incubated overnight at 4°C with rotation with 20 µg/ml anti-FLAG M2 antibody (Merck, F3165) and 50 µl Pierce magnetic protein A/G beads (Thermo Fisher Scientific) pre-washed with KHM buffer. Beads were collected on a magnetic rack and washed 3x with 500 µl KHM buffer and 1x with PBS (with protease inhibitors) and then resuspended in PBS containing 1 mg/ml BSA. hSARM1-Flag concentration in the bead suspension was determined relative to an hSARM1 standard (purified from Drosophila Schneider 2 cells) by immunoblotting using a rabbit polyclonal antibody raised against human SAM-TIR.

hSARM1 NADase activity

Rates of NAD consumption by recombinant hSARM1 were measured by HPLC under a discontinuous assay that was set as follows. Typically, mixtures of 0.02-0.2 ml

contained 2-20 µg/ml of hSARM1-Flag (on-beads) in buffer HEPES/NaOH 50 mM, pH 7.5, and 250 µM of the substrate NAD. NMN, VMN and VAD were added at the concentrations indicated in the figures. Reactions were initiated by adding NAD, incubated at 25 °C in a water-bath, stopped at appropriate times by $HClO_4$ treatment, neutralised with K_2CO_3, and subsequently analysed by ion-pair reverse-phase (RP) HPLC (NAM, NMN, NAD, ADPR, cADPR) [28] or under optimised conditions for VMN and VAD detection [19]. The products formed (NAM, ADPR and cADPR) were quantified from the area of separated peaks. Rates were calculated under NAD consumption ≤ 20% from the linearly accumulating products ADPR and cADPR (Fig. S5b). One unit (U) of activity represents the enzyme amount that forms 1 µmol/min of the products above under these assay conditions. Data from three independent experiments were averaged to calculate hSARM1 activity fold activation (Fig. 3c) and then studied by fitting through the Excel software package to the rate equation below

$$V = \frac{V_{max}\left(X + \left(\frac{1-X}{1+\left(\frac{[I]}{K_a}\right)^n}\right)\right)\left(Y + \left(\frac{1-Y}{1+\left(\frac{[I]}{K_i}\right)^n}\right)\right)[S]}{K_m + [S]}$$

that represents a Michaelis-Menten equation adapted to be valid for readily reversible effectors, *i.e.* including activators and inhibitors binding via distinct sites to one protein target. Maximum velocity (V_{max}) represents the rate in the absence of the effector (basal activity) corrected by the two parameters between parentheses, the first for activation and the second for inhibition, taking into account opposite and independent contributions exerted by the single but dual effector I. *X* is the "relative activity fold" factor at varying concentrations of I, *Y* is the residual activity fraction at saturating

concentration of I, K_a is the affinity constant of I for the activation site, K_i is the affinity constant of I for the inhibition site, and n is the Hill coefficient indicating cooperativity (if ≠ 1).

NMN deamidase activity

Recombinant *E. coli* NMN deamidase was obtained as previously described [32]. Activity was measured in buffer HEPES/NaOH 50 mM, pH 7.5, in the presence of 4 milliU/ml enzyme, 0.5 mg/ml BSA, and 250 µM NMN or VMN. Vacor, VMN and VAD, all at the concentration of 250 µM, were also assayed in presence of the substrate NMN. Reactions were incubated at 37 °C, then stopped and analysed by HPLC using the two methods described above [19,28]. The NMN deamidase rates were calculated after separation and quantification of the NaMN product formed from NMN, and finally reported as relative percentages of controls in the presence of NMN alone.

Western blot

Following treatment with vacor, DRG ganglia were separated from their neurites with a scalpel. Neurites and ganglia were collected, washed in ice-cold PBS containing protease inhibitors (Roche), and lysed directly in 15 µl 2x Laemmli buffer containing 10% 2-Mercaptoethanol (Merck). Samples were loaded on a 4-to-20% SDS polyacrylamide gel (Bio-Rad). Membranes were blocked for 3 hr in 5% milk in TBS (50 mM Trizma base and 150 mM NaCl, PH 8.3, both Merck) plus 0.05% Tween-20 (Merck) (TBST), incubated overnight with primary antibody in 5% milk in TBST at 4°C and subsequently washed in TBST and incubated for 1 hr at room temperature with HRP-linked secondary antibody (Bio-Rad) in 5% milk in TBST. Membranes were washed, treated with SuperSignal™ West Dura Extended Duration Substrate (Thermo Fisher Scientific) and imaged with Uvitec Alliance imaging system. The following primary antibodies were used: mouse monoclonal anti-SARM1 [27] (1:5000) and mouse

anti-β-actin (Merck, A5316, 1:2000) as a loading control. Quantification of band intensity was determined by densitometry using ImageJ.

Statistical analysis

Statistical testing of data was performed using Prism (GraphPad Software, La Jolla, USA). The appropriate tests used and the n numbers of each individual experiment are described in the figure legends. A p-value < 0.05 was considered significant.

AUTHOR CONTRIBUTIONS

A.L., G.O. and M.P.C conceived the study. A.L. designed and performed all experiments on neurons, with help from E.M.. C.A. and G.O. designed and performed nucleotide measurements and biochemical assays, with help from A.A.. J.G. contributed to the interpretation of the results and developed the hSARM1 purification protocol, with help from L.M.D.. P.A-F. and W.Q. contributed to the interpretation of the results. A.L. and M.P.C. wrote the manuscript, with input from J.G. and G.O. All authors read and approved the manuscript.

ACKNOWLEDGMENTS

We thank members of the Coleman lab and Prof Nadia Raffaelli for useful discussions. We also thank Dr Lucia Silvestrini for help in obtaining the Neurospora crassa NADase for the cADPR detection assay. This work was funded by a Sir Henry Wellcome postdoctoral fellowship from the Wellcome Trust [grant number 210904/Z/18/Z], a Wellcome Trust Clinical Research Career Development Fellowship [Grant/Award Number: 206634]; BBSRC/AstraZeneca Industrial Partnership Award BB/S009582/1 and Grants RSA 2016-18 and 2017-19 from UNIVPM.

COMPETING INTERESTS STATEMENT

This work is in part funded by a BBSRC/AstraZeneca Industrial Partnership Award and Q.W. and L.M.D. were employees of AstraZeneca for part of the project.

REFERENCES

1. Osterloh, J. M. *et al.* dSarm/Sarm1 is required for activation of an injury-induced axon death pathway. *Science* **337**, 481–484 (2012).
2. Coleman, M. P. & Höke, A. Programmed axon degeneration: from mouse to mechanism to medicine. *Nat. Rev. Neurosci.* **21**, 183–196 (2020).
3. Huppke, P. *et al.* Homozygous NMNAT2 mutation in sisters with polyneuropathy and erythromelalgia. *Exp. Neurol.* **320**, 112958 (2019).
4. Lukacs, M. *et al.* Severe biallelic loss-of-function mutations in nicotinamide mononucleotide adenylyltransferase 2 (NMNAT2) in two fetuses with fetal akinesia deformation sequence. *Exp. Neurol.* **320**, 112961 (2019).
5. Essuman, K. *et al.* The SARM1 Toll/Interleukin-1 Receptor Domain Possesses Intrinsic NAD+ Cleavage Activity that Promotes Pathological Axonal Degeneration. *Neuron* **93**, 1334-1343.e5 (2017).
6. Gilley, J. & Coleman, M. P. Endogenous Nmnat2 Is an Essential Survival Factor for Maintenance of Healthy Axons. *PLOS Biol.* **8**, e1000300 (2010).
7. Gilley, J., Orsomando, G., Nascimento-Ferreira, I. & Coleman, M. P. Absence of SARM1 Rescues Development and Survival of NMNAT2-Deficient Axons. *Cell Rep.* **10**, 1974–1981 (2015).
8. Sasaki, Y., Nakagawa, T., Mao, X., DiAntonio, A. & Milbrandt, J. NMNAT1 inhibits axon degeneration via blockade of SARM1-mediated NAD+ depletion. *eLife* https://elifesciences.org/articles/19749 (2016) doi:10.7554/eLife.19749.
9. Sasaki, Y. *et al.* cADPR is a gene dosage-sensitive biomarker of SARM1 activity in healthy, compromised, and degenerating axons. *Exp. Neurol.* 113252 (2020) doi:10.1016/j.expneurol.2020.113252.
10. Di Stefano, M. *et al.* A rise in NAD precursor nicotinamide mononucleotide (NMN) after injury promotes axon degeneration. *Cell Death Differ.* **22**, 731–742 (2015).
11. Di Stefano, M. *et al.* NMN Deamidase Delays Wallerian Degeneration and Rescues Axonal Defects Caused by NMNAT2 Deficiency In Vivo. *Curr. Biol.* **27**, 784–794 (2017).

12. Loreto, A., Di Stefano, M., Gering, M. & Conforti, L. Wallerian Degeneration Is Executed by an NMN-SARM1-Dependent Late Ca2+ Influx but Only Modestly Influenced by Mitochondria. *Cell Rep.* **13**, 2539–2552 (2015).
13. Loreto, A. *et al.* Mitochondrial impairment activates the Wallerian pathway through depletion of NMNAT2 leading to SARM1-dependent axon degeneration. *Neurobiol. Dis.* **134**, 104678 (2020).
14. Zhao, Z. Y. *et al.* A Cell-Permeant Mimetic of NMN Activates SARM1 to Produce Cyclic ADP-Ribose and Induce Non-apoptotic Cell Death. *iScience* **15**, 452–466 (2019).
15. Gilley, J., Ribchester, R. R. & Coleman, M. P. Sarm1 Deletion, but Not WldS, Confers Lifelong Rescue in a Mouse Model of Severe Axonopathy. *Cell Rep.* **21**, 10–16 (2017).
16. Gallanosa, A. G., Spyker, D. A. & Curnow, R. T. Diabetes Mellitus Associated with Autonomic and Peripheral Neuropathy after Vacor Rodenticide Poisoning: A Review. *Clin. Toxicol.* **18**, 441–449 (1981).
17. LeWitt, P. A. The Neurotoxicity of the Rat Poison Vacor. *N. Engl. J. Med.* **302**, 73–77 (1980).
18. Watson, D. F. & Griffin, J. W. Vacor Neuropathy: Ultrastructural and Axonal Transport Studies. *J. Neuropathol. Exp. Neurol.* **46**, 96–108 (1987).
19. Buonvicino, D. *et al.* Identification of the Nicotinamide Salvage Pathway as a New Toxification Route for Antimetabolites. *Cell Chem. Biol.* **25**, 471-482.e7 (2018).
20. Gerdts, J., Summers, D. W., Sasaki, Y., DiAntonio, A. & Milbrandt, J. Sarm1-Mediated Axon Degeneration Requires Both SAM and TIR Interactions. *J. Neurosci.* **33**, 13569–13580 (2013).
21. Gerdts, J., Brace, E. J., Sasaki, Y., DiAntonio, A. & Milbrandt, J. SARM1 activation triggers axon degeneration locally via NAD^+ destruction. *Science* **348**, 453–457 (2015).
22. Bratkowski, M. *et al.* Structural and Mechanistic Regulation of the Pro-degenerative NAD Hydrolase SARM1. *Cell Rep.* **32**, 107999 (2020).
23. Horsefield, S. *et al.* NAD+ cleavage activity by animal and plant TIR domains in cell death pathways. *Science* **365**, 793–799 (2019).

24. Sporny, M. *et al.* Structural Evidence for an Octameric Ring Arrangement of SARM1. *J. Mol. Biol.* **431**, 3591–3605 (2019).
25. Sporny, M. *et al.* The Structural Basis for SARM1 Inhibition, and Activation Under Energetic Stress.bioRxiv. https://www.biorxiv.org/content/10.1101/2020.08.05.238287v1.
26. Sasaki, Y., Vohra, B. P. S., Lund, F. E. & Milbrandt, J. Nicotinamide Mononucleotide Adenylyl Transferase-Mediated Axonal Protection Requires Enzymatic Activity But Not Increased Levels of Neuronal Nicotinamide Adenine Dinucleotide. *J. Neurosci. Off. J. Soc. Neurosci.* **29**, 5525–5535 (2009).
27. Chen, C.-Y., Lin, C.-W., Chang, C.-Y., Jiang, S.-T. & Hsueh, Y.-P. Sarm1, a negative regulator of innate immunity, interacts with syndecan-2 and regulates neuronal morphology. *J. Cell Biol.* **193**, 769–784 (2011).
28. Mori, V. *et al.* Metabolic Profiling of Alternative NAD Biosynthetic Routes in Mouse Tissues. *PLOS ONE* **9**, e113939 (2014).
29. Graeff, R. & Lee, H. C. A novel cycling assay for cellular cADP-ribose with nanomolar sensitivity. *Biochem. J.* **361**, 379–384 (2002).
30. Amici, A. *et al.* Synthesis and Degradation of Adenosine 5′-Tetraphosphate by Nicotinamide and Nicotinate Phosphoribosyltransferases. *Cell Chem. Biol.* **24**, 553-564.e4 (2017).
31. Orsomando, G. *et al.* Simultaneous Single-Sample Determination of NMNAT Isozyme Activities in Mouse Tissues. *PLOS ONE* **7**, e53271 (2012).
32. Zamporlini, F. *et al.* Novel assay for simultaneous measurement of pyridine mononucleotides synthesizing activities allows dissection of the NAD+ biosynthetic machinery in mammalian cells. *FEBS J.* **281**, 5104–5119 (2014).